Available online at www.sciencedirect.com

ScienceDirect

International Journal of Solids and Structures 45 (2008) 1935–1953

INTERNATIONAL JOURNAL OF SOLIDS AND STRUCTURES

www.elsevier.com/locate/ijsolstr

Crack energy density in arbitrary direction for piezoelectrics and its characteristic features in electromechanical mixed mode crack

Byeung-Gun Nam *, Katsuhiko Watanabe

Institute of Industrial Science, The University of Tokyo, 4-6-1, Komaba, Meguro-ku, Tokyo 153-8505, Japan

Received 18 June 2007; received in revised form 25 August 2007
Available online 13 November 2007

Abstract

The concepts of crack energy density (CED) and its derivatives in arbitrary direction were established for piezoelectric material and, keeping their application to mixed mode fracture in mind, the characteristic features of them as fracture parameters were investigated based on the approximate equations for CED and its derivatives. That is, CED and its derivatives in arbitrary direction are defined first and separation into their each mode contribution is made. Subsequently, path independent integral expressions of them are derived, and then using them, approximate equations of each mode contribution of CED are obtained concretely for the case where linear singular solution is known. The resulting equations are then used to investigate the effects of electric field and electrical boundary condition on CED and its derivatives. An infinite piezoelectric plane with a crack inclined with respect to the poling direction is considered as a numerical example. Mode I contribution of mechanical CED is mainly employed as a possible fracture parameter for the study and it was shown that applied electric field significantly influences on fracture parameters especially for the impermeable crack perpendicular to the poling direction. The effect of electric field has the tendency to decrease as crack inclination angle increases. It was also found that, even for the impermeable crack perpendicular to the poling direction, crack propagation could be deviated from self-similar direction under a strong negative electric field, and this fact is qualitatively consistent with an existing experimental observation. For the ideally sharp crack with no width, impermeable and Hao and Shen type boundary conditions are admissible showing qualitative agreement with experimental results, but exact boundary condition is not suitable and finally consistent with permeable boundary condition.

Keywords: Piezoelectric material; Crack energy density (CED) in arbitrary direction; Mixed mode crack; Electric boundary condition

1. Introduction

With more increasing use of piezoelectric ceramics in smart devices like sensors and actuators, the concerns about their reliability for strength and fracture have been growing in recent years. Over the past two decades, a considerable number of studies have been made on fracture of piezoelectric materials and many of them have

* Corresponding author. Tel.: +81 3 5452 6128; fax: +81 3 5452 6129.
E-mail address: nam@iis.u-tokyo.ac.jp (B.-G. Nam).

0020-7683/$ - see front matter © 2007 Elsevier Ltd. All rights reserved.
doi:10.1016/j.ijsolstr.2007.11.002

especially focused on the influence of applied electric fields on crack strength. However, there has been little agreement even on the fracture parameter itself and their fracture mechanism is still controversial.

Considering the fact that most defects existing in piezoelectric devices are not simply in mode I condition but mainly in so-called mixed mode condition, studies on the crack behavior under mixed mode are indispensable for the materials. Nonetheless, very few attempts have been made at the electromechanical mixed mode fracture and the knowledge of the issue is surprisingly limited. As examples, McHenry and Koepke (1983) first observed that crack propagation could be deviated from its original direction under a strong electric field. Three-point bending specimen with an unsymmetrical crack was adopted for mixed mode fracture test and fracture initiation loads and directions were measured (Park and Sun, 1995). Xu and Rajapakse (1999) derived analytical crack tip singular fields for a piezoelectric plane with an arbitrarily oriented elliptical void. They extended the solutions further by removing the commonly used assumptions that the void boundary condition is impermeable (Xu and Rajapakse, 2001). Recently, their result was applied in order to obtain the expression of strain energy density factor under assumption of impermeable crack surface boundary condition (Chue and Weng, 2005). However, the governing fracture parameter is still ambiguous even for a mode I crack of which the extension is supposed to be self-similar, and we must say that it is more ambiguous for a mixed mode crack that leads to non-self-similar crack extension.

For a mode I crack that causes self-similar extension crack, we newly defined crack energy density (hereafter CED) for piezoelectric materials as a possible fracture parameter and clarified some fundamental matters such as its meaning, relation to other fracture parameters and loading path dependency (Nam and Watanabe, 2007). Also the CED for the case where a defect filled with an electric inclusion exists was discussed and the effect of the electric boundary condition on CED was investigated through finite element analyses (Nam and Watanabe, 2008). Moreover, we proposed a fracture criterion that a crack starts to grow when the mechanical contribution of CED reaches a certain critical value peculiar to the material and its applicability was also demonstrated through the comparison between experimental and numerical results (Nam et al., 2007).

Keeping a mixed mode crack in mind, in this work, the concept of CED defined as the quantity in the crack direction is extended to the quantity meaningful also in an arbitrary direction. That is, the CED in an arbitrary direction for piezoelectric material is defined first. Then, separation of its each mode contribution is conducted and path independent integral expressions of CED in arbitrary direction and its derivatives, including its each mode contribution, are then derived. For a linear electro-elastic piezoelectric material with an arbitrarily oriented crack to poling direction, approximate equations of CED and its derivatives will be derived based on some assumption and using the singular solutions by Xu and Rajapakse (2001). Finally, paying our attention mainly to mode I contribution of mechanical part of CED in an arbitrary direction as a possible fracture parameter, the influence of applied electric fields on them and crack growth direction are examined, varying the electric boundary condition on crack surface, based on the approximate equations.

2. CED in arbitrary direction for piezoelectrics

In this section, based on the knowledge obtained in the previous papers for the case where self-similar crack extension is supposed (Nam and Watanabe, 2007, 2008), CED in arbitrary direction is discussed taking crack extension in the corresponding direction into account. First, the definition of CED in arbitrary direction is given. Then, the path independent expressions of CED in arbitrary direction and its derivative are derived.

2.1. Definition

Consider a piezoelectric medium containing a notch-like crack with sufficiently small root radius ρ as shown in Fig. 1. The crack is supposed to be filled with a dielectric inclusion such as air or vacuum. In figure, (X_1, X_2, X_3) is a fixed coordinate and (x_1, x_2, x_3) is a coordinate which is given by rotating (X_1, X_2, X_3) by the amount of φ around X_3-axis. $\Gamma^+(0)$ and $\Gamma^-(0)$ are the parts of semi-circular path along crack (notch) tip in $x_1 \geqslant 0$ and $x_1 \leqslant 0$, respectively. Call, hereafter, the shaded thin layer between two broken lines parallel to x_1 axis, that becomes a plane in the limit when ρ approaches 0, just φ *plane*, for descriptive purposes. Then, as in the case of ordinary materials (Watanabe and Shiomi (1984); Utsunomiya (1992)), the CED in arbitrary direction (in x_1 direction), $\mathcal{E}_\varphi$, for piezoelectric materials can be defined by

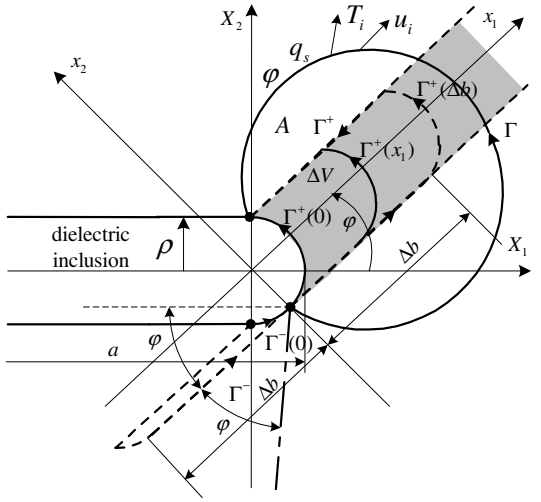

Fig. 1. A notch-like crack filled with a dielectric inclusion.

$$\mathcal{E}_\varphi = \lim_{\Delta b\to 0}\left(\int_{\Delta V} W\,\mathrm{d}V\right)\Big/\Delta b = \lim_{\Delta b\to 0}\int_0^{\Delta b}\left(\int_{\Gamma^+(x_1)} W\,\mathrm{d}x_2\right)\mathrm{d}x_1\Big/\Delta b = \int_{\Gamma^+(0)} W\,\mathrm{d}x_2 \tag{1}$$

and this physically means *the work, expressed per unit area in the φ plane, done at the $\Gamma^+(0)$ part of the crack tip during electromechanical deformation.* Here, ΔV is the volume of the shaded layer, of which the length in x_1 direction is Δb, between, letting $\Gamma^+(x_1)$ be the path obtained by moving $\Gamma^+(0)$ in parallel by $x_1(\geqslant 0)$, $\Gamma^+(0)$ and $\Gamma^+(\Delta b)$ in Fig. 1. Unit thickness is considered in the direction of thickness (in x_3 direction). W is the quantity, which may be called extended strain energy density, defined by

$$\begin{aligned} W &= W^{\mathrm{M}} + W^{\mathrm{E}} \\ W^{\mathrm{M}} &= \int_0^t \sigma_{ij}\mathrm{d}\varepsilon_{ij}, \quad W^{\mathrm{E}} = \int_0^t E_i \mathrm{d}D_i \end{aligned} \tag{2}$$

where σ_{ij}, ε_{ij}, D_i and E_i are stress, strain, electric displacement and electric field components defined in (x_1, x_2, x_3) coordinate, respectively. Note that the subscripts of tensors and vectors, i and j, in this work are based on (x_1, x_2, x_3) coordinate hereafter. Superscripts M and E denote mechanical and electrical parts for the corresponding quantities, respectively. The integral means to integrate from time $\tau = 0$ for initial state to present time $\tau = t$ along actual loading path and the same goes for hereafter. $\mathcal{E}_\varphi$ by Eq. (1) is the natural extension of the definition of CED formerly given considering self-similar crack extension (Nam and Watanabe, 2007) and $\mathcal{E}_\varphi$ when $\varphi = 0^\circ$ naturally coincides with it. $\mathcal{E}_\varphi$ is the quantity that may be called *strain energy area density* in the φ plane to which our attention is paid.

Since W is defined as the sum of its mechanical contribution W^{M} and electrical contribution W^{E}, as shown in Eq. (2), $\mathcal{E}_\varphi$ can be divided into its mechanical part $\mathcal{E}_\varphi^{\mathrm{M}}$ and electrical part $\mathcal{E}_\varphi^{\mathrm{E}}$. Moreover, it is shown for ordinary materials that CED in arbitrary direction can be divided into each deformation mode contribution in general (Utsunomiya, 1992), and $\mathcal{E}_\varphi^{\mathrm{M}}$ and $\mathcal{E}_\varphi^{\mathrm{E}}$ for piezoelectric materials are also divided into each mode contribution in the same manner without loss of generality. That is, when in-plane problem is considered,

$$\begin{aligned} \mathcal{E}_\varphi &= \mathcal{E}_\varphi^{\mathrm{M}} + \mathcal{E}_\varphi^{\mathrm{E}} \\ \mathcal{E}_\varphi^{\mathrm{M}} &= \int_{\Gamma^+(0)} W^{\mathrm{M}}\mathrm{d}x_2, \quad \mathcal{E}_\varphi^{\mathrm{E}} = \int_{\Gamma^+(0)} W^{\mathrm{E}}\mathrm{d}x_2 \\ \mathcal{E}_\varphi^{\mathrm{M}} &= \mathcal{E}_\varphi^{\mathrm{MI}} + \mathcal{E}_\varphi^{\mathrm{MII}} \end{aligned}$$

$$\begin{aligned}
\mathcal{E}_{\varphi}^{\mathrm{MI}} &= \int_{\Gamma^{+}(0)} W^{\mathrm{MI}}\mathrm{d}x_2, \quad \mathcal{E}_{\varphi}^{\mathrm{MII}} = \int_{\Gamma^{+}(0)} W^{\mathrm{MII}}\mathrm{d}x_2 \\
\mathcal{E}_{\varphi}^{\mathrm{E}} &= \mathcal{E}_{\varphi}^{\mathrm{EI}} + \mathcal{E}_{\varphi}^{\mathrm{EII}} \\
\mathcal{E}_{\varphi}^{\mathrm{EI}} &= \int_{\Gamma^{+}(0)} W^{\mathrm{EI}}\mathrm{d}x_2, \quad \mathcal{E}_{\varphi}^{\mathrm{EII}} = \int_{\Gamma^{+}(0)} W^{\mathrm{EII}}\mathrm{d}x_2
\end{aligned} \tag{3}$$

where superscripts I and II denote mode I and mode II contributions of each quantity, respectively.

The CED in arbitrary direction (in x_1 direction) for the crack model of $\rho = 0$ is defined, as the limit when ρ approaches zero, by

$$\mathcal{E}_{\varphi}^{(\mathrm{c})} = \lim_{\rho \to 0} \int_{\Gamma^{+}(0)} W\,\mathrm{d}x_2 \tag{4}$$

The same thing goes also for other quantities. The superscript (c) is attached here just to show that it is the quantity defined for the crack model of $\rho = 0$. Hereafter, also when the case of $\rho = 0$ is considered, the superscript will not be attached for simplicity, because the case can be dealt with as the limit of the case for a notch.

Also the complementary quantities of the CED above can be defined in the similar way and, for a later use, define the complementary quantity of $\mathcal{E}_{\varphi}^{\mathrm{E}}$ by

$$\mathcal{E}_{\varphi\mathrm{c}}^{\mathrm{E}} = \int_{\Gamma^{+}(0)} W_{\mathrm{c}}^{\mathrm{E}}\mathrm{d}x_2, \quad W_{\mathrm{c}}^{\mathrm{E}} = \int_0^t D_i \mathrm{d}E_i \tag{5}$$

where, subscript c denotes the complementary quantity and the same goes hereafter. It goes without saying that $\mathcal{E}_{\varphi\mathrm{c}}^{\mathrm{E}}$ has the meaning of electrical contribution of the complementary energy area density.

Here, consider the case where the positive direction of x_1 axis is reversed, that is, the rotation angle of x_1 and x_2 axes is $\varphi'(= \varphi - 180^\circ)$ as shown in Fig. 2 (when $\varphi < 0^\circ$, obviously $\varphi' = \varphi + 180^\circ$). Also in this case, CED in x_1 direction is defined, corresponding to Eq. (1), by

$$\mathcal{E}_{\varphi'} = \int_{\Gamma_{\varphi'}^{+}(0)} W\,\mathrm{d}x_2 \tag{6}$$

When the notation here is used, $\Gamma^{+}(0)$ in Eq. (1) and Fig. 1 should be expressed by $\Gamma_{\varphi}^{+}(0)$. However, subscript φ of Γ is omitted in Eq. (1) and Fig. 1 for simplicity and the same goes also hereafter. Considering that $\Gamma_{\varphi'}^{+}(0)$ and $\mathrm{d}x_2$ in Fig. 2 correspond to $\Gamma^{-}(0)$ and $-\mathrm{d}x_2$ in Fig. 1, respectively, the CED in the φ' plane can be expressed also by

$$\mathcal{E}_{\varphi'} = -\int_{\Gamma^{-}(0)} W\,\mathrm{d}x_2 \tag{7}$$

It should be noted that $\Gamma^{-}(0)$ in Fig. 1 is related to the CED in the opposite direction.

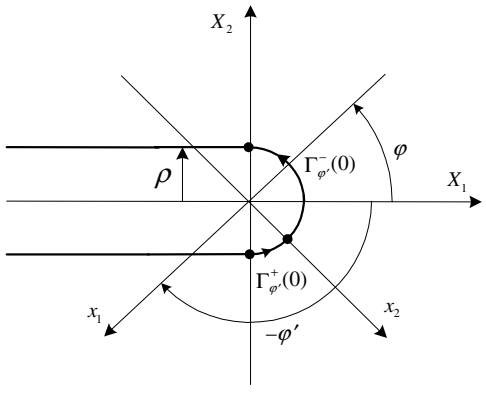

Fig. 2. A coordinate system rotated by the amount of $\varphi - 180^\circ$ with respect to X_3-axis.

2.2. Path independent integral expressions

Consider again the piezoelectric medium subjected to electromechanical loads shown in Fig. 1. Let Γ be an arbitrary path surrounding the path $\Gamma^+(0)$ and A be the area surrounded by closed path $\Gamma - \Gamma^+(0)$. Body force and free charge are not considered for simplicity. Then, the following electromechanical energy conservation law generally holds (Nam and Watanabe, 2007):

$$\int_{\Gamma-\Gamma^+(0)} (Wn_1 - T_i u_{i,1} - \phi q_{s,1})\mathrm{d}\Gamma - \int_A \int_0^t (\sigma_{ij,1}\mathrm{d}\varepsilon_{ij} - \varepsilon_{ij,1}d\sigma_{ij} + E_{j,1}dD_j - D_{j,1}\mathrm{d}E_j)\,\mathrm{d}A = 0 \tag{8}$$

Here, T_i, u_i, ϕ and q_s are traction, displacement, electric potential and surface charge, respectively; n_i is outward unit normal vector. Therefore, taking Eq. (1) and $T_i = 0$ on $\Gamma^+(0)$ into consideration, the relation as

$$\begin{aligned}\mathcal{E}_\varphi = \int_{\Gamma^+(0)} W\mathrm{d}x_2 &= \int_{\Gamma^+(0)} \phi q_{s,1}\mathrm{d}\Gamma + \int_\Gamma (Wn_1 - T_i u_{i,1} - \phi q_{s,1})\mathrm{d}\Gamma \\ &- \int_A \int_0^t (\sigma_{ij,1}\mathrm{d}\varepsilon_{ij} - \varepsilon_{ij,1}\mathrm{d}\sigma_{ij} + E_{j,1}\mathrm{d}D_j - D_{j,1}dE_j)\,\mathrm{d}A\end{aligned} \tag{9}$$

is derived from Eq. (8). Moreover, as the conservation laws similar to Eq. (8) hold for each of mechanical, electrical and its complementary quantities (Nam and Watanabe, 2007), also the relations as

$$\mathcal{E}^{\mathrm{M}}_\varphi = \int_{\Gamma^+(0)} W^{\mathrm{M}}\mathrm{d}x_2 = \int_\Gamma (W^{\mathrm{M}}n_1 - T_i u_{i,1})\mathrm{d}\Gamma - \int_A \int_0^t (\sigma_{ij,1}\mathrm{d}\varepsilon_{ij} - \varepsilon_{ij,1}\mathrm{d}\sigma_{ij})\,\mathrm{d}A \tag{10}$$

$$\mathcal{E}^{\mathrm{E}}_\varphi = \int_{\Gamma^+(0)} W^{\mathrm{E}}\mathrm{d}x_2 = \int_{\Gamma^+(0)} \phi q_{s,1}\mathrm{d}\Gamma + \int_\Gamma (W^{\mathrm{E}}n_1 - \phi q_{s,1})\mathrm{d}\Gamma - \int_A \int_0^t (E_{j,1}\mathrm{d}D_j - D_{j,1}\mathrm{d}E_j)\,\mathrm{d}A \tag{11}$$

$$\mathcal{E}^{\mathrm{E}}_{\varphi\mathrm{c}} = \int_{\Gamma^+(0)} W^{\mathrm{E}}_{\mathrm{c}}\mathrm{d}X_2 = \int_{\Gamma^+(0)} q_s\phi_{,1}\mathrm{d}\Gamma + \int_\Gamma (W^{\mathrm{E}}_{\mathrm{c}}n_1 - q_s\phi_{,1})\mathrm{d}\Gamma + \int_A \int_0^t (E_{j,1}\mathrm{d}D_j - D_{j,1}\mathrm{d}E_j)\,\mathrm{d}A \tag{12}$$

are derived from these conservation laws.

$\mathcal{E}_\varphi$, $\mathcal{E}^{\mathrm{M}}_\varphi$, $\mathcal{E}^{\mathrm{E}}_\varphi$ and $\mathcal{E}^{\mathrm{E}}_{\varphi\mathrm{c}}$ can be separated into each mode contribution in the same manner as for ordinary materials. Although just the results are shown here, when path Γ is taken, letting the dashed-dotted line in Fig. 1 be a boundary line, so as to go through only in the region that includes ΔV, the path integral expressions of their each mode contribution can be given as

$$\begin{aligned}\mathcal{E}^{\alpha}_\varphi = \int_{\Gamma^+(0)} W^{\alpha}\mathrm{d}x_2 &= \int_{\Gamma^+(0)} \phi^{\alpha} q^{\alpha}_{s,1}\mathrm{d}\Gamma + \int_\Gamma (W^{\alpha}n_1 - T^{\alpha}_i u^{\alpha}_{i,1} - \phi^{\alpha} q^{\alpha}_{s,1})\,\mathrm{d}\Gamma \\ &- \int_A \int_0^t (\sigma^{\alpha}_{ij,1}\mathrm{d}\,\varepsilon^{\alpha}_{ij} - \mathcal{E}^{\alpha}_{ij,1}\mathrm{d}\,\sigma^{\alpha}_{ij} + E^{\alpha}_{j,1}\mathrm{d}\,D^{\alpha}_j - D^{\alpha}_{j,1}\mathrm{d}\,E^{\alpha}_j)\,\mathrm{d}A\end{aligned} \tag{13}$$

$$\mathcal{E}^{\mathrm{M}\alpha}_\varphi = \int_{\Gamma^+(0)} W^{\mathrm{M}\alpha}\mathrm{d}x_2 = \int_\Gamma (W^{\mathrm{M}\alpha}n_1 - T^{\alpha}_i u^{\alpha}_{i,1})\mathrm{d}\Gamma - \int_A \int_0^t (\sigma^{\alpha}_{ij,1}\mathrm{d}\,\varepsilon^{\alpha}_{ij} - \varepsilon^{\alpha}_{ij,1}\mathrm{d}\,\sigma^{\alpha}_{ij})\,\mathrm{d}A \tag{14}$$

$$\mathcal{E}^{\mathrm{E}\alpha}_\varphi = \int_{\Gamma^+(0)} W^{\mathrm{E}\alpha}\mathrm{d}x_2 = \int_{\Gamma^+(0)} \phi^{\alpha} q^{\alpha}_{s,1}\mathrm{d}\Gamma + \int_\Gamma (W^{\mathrm{E}\alpha}n_1 - \phi^{\alpha} q^{\alpha}_{s,1})\mathrm{d}\Gamma - \int_A \int_0^t (E^{\alpha}_{j,1}\mathrm{d}\,D^{\alpha}_j - D^{\alpha}_{j,1}\mathrm{d}\,E^{\alpha}_j)\,\mathrm{d}A \tag{15}$$

$$\mathcal{E}^{\mathrm{E}\alpha}_{\varphi\mathrm{c}} = \int_{\Gamma^+(0)} W^{\mathrm{E}\alpha}_{\mathrm{c}}\mathrm{d}X_2 = \int_{\Gamma^+(0)} q^{\alpha}_s\phi^{\alpha}_{,1}\mathrm{d}\Gamma + \int_\Gamma (W^{\mathrm{E}\alpha}_{\mathrm{c}}n_1 - q^{\alpha}_s\phi^{\alpha}_{,1})\mathrm{d}\Gamma + \int_A \int_0^t (E^{\alpha}_{j,1}\mathrm{d}\,D^{\alpha}_j - D^{\alpha}_{j,1}\mathrm{d}\,E^{\alpha}_j)\,\mathrm{d}A \tag{16}$$

Generally, as a concrete example is shown in Section 3.1, the quantity is divided into the component that become symmetric about x_1–x_3 plane when $\rho \to 0$ and the component that becomes anti-symmetric about x_1–x_3 plane when $\rho \to 0$, and the former contributes to mode I deformation and the latter to mode II deformation (Utsunomiya, 1992). In these equations, superscript α (=I and II) is used to denote each mode contribution for corresponding quantities. In Eqs. (9)–(16), path Γ in the integrals of the right-hand sides can be taken arbitrarily (although, in case of Eqs. (13)–(16), the region where the path Γ can be taken is limited as mentioned above), thus we may call them path independent integrals.

The constitutive relation under isentropic process, provided that material behavior is reversible, is given by

$$\sigma_{ij} = \frac{\partial U}{\partial \varepsilon_{ij}}, \quad E_i = \frac{\partial U}{\partial D_i} \tag{17}$$

Here, U is internal energy density. In this case, the integrand of area integral term in Eq. (9) becomes zero (Nam and Watanabe, 2007), that is,

$$\sigma_{ij,1}\mathrm{d}\,\varepsilon_{ij} - \varepsilon_{ij,1}\mathrm{d}\,\sigma_{ij} + E_{i,1}\mathrm{d}\,D_i - D_{i,1}\mathrm{d}\,E_i = 0 \tag{18}$$

Therefore, Eq. (9) can be rewritten as

$$\mathcal{E}_\varphi = \int_{\Gamma^+(0)} W\,\mathrm{d}\,x_2 = \int_{\Gamma^+(0)} \phi q_{s,1}\mathrm{d}\Gamma + \int_\Gamma (Wn_1 - T_i u_{i,1} - \phi q_{s,1})\mathrm{d}\Gamma \tag{19}$$

As for the integrand of area integral term in Eq. (13), note that the same holds true only for linear electroelastic case where the principle of superposition holds and the relation corresponding to Eq. (17) exists. The area integral terms in Eqs. (14) and (15) do not vanish generally even under linear assumption, contrary to that in Eq. (13). This means that, as was the case for $\mathcal{E}_\varphi^{\mathrm{M}}$, $\mathcal{E}_\varphi^{\mathrm{E}}$ and $\mathcal{E}_{\varphi\mathrm{c}}^{\mathrm{E}}$ when $\varphi = 0^\circ$ (Nam and Watanabe, 2007), $\mathcal{E}_\varphi^{\mathrm{M}\alpha}$ and $\mathcal{E}_\varphi^{\mathrm{E}\alpha}$ as well as $\mathcal{E}_\varphi^{\mathrm{M}}$, $\mathcal{E}_\varphi^{\mathrm{E}}$ and $\mathcal{E}_{\varphi\mathrm{c}}^{\mathrm{E}}$ are dependent, in general, on electromechanical loading history from the beginning to the present time.

Γ in Fig. 1 is an arbitrary path surrounding the path $\Gamma^+(0)$, thus let us take the path Γ^+, which partly includes path $\Gamma^+(\Delta b)$, denoted by dotted line as Γ. The area enclosed by $\Gamma^+ - \Gamma^+(0)$ is denoted by A_ρ. Then, since the contribution of $\Gamma^+(\Delta b)$ vanishes when ρ approaches 0 and n_1 equals to 0 on upper and lower surfaces of Γ^+, Eqs. (10)–(12) can be rewritten, respectively, as

$$\mathcal{E}_\varphi^{\mathrm{M}} = \lim_{\rho\to 0}\int_{\Gamma^+} (-T_i u_{i,1})\mathrm{d}\Gamma - \lim_{\rho\to 0}\int_{A_\rho}\int_0^t (\sigma_{ij,1} d\varepsilon_{ij} - \varepsilon_{ij,1}\mathrm{d}\,\sigma_{ij})\mathrm{d}A \tag{20}$$

$$\mathcal{E}_\varphi^{\mathrm{E}} = \lim_{\rho\to 0}\int_{\Gamma^+(0)} \phi q_{s,1}\mathrm{d}\Gamma + \lim_{\rho\to 0}\int_{\Gamma^+} (-\phi q_{s,1})\mathrm{d}\Gamma - \lim_{\rho\to 0}\int_{A_\rho}\int_0^t (E_{j,1}\mathrm{d}\,D_j - D_{j,1}\mathrm{d}\,E_j)\mathrm{d}A \tag{21}$$

$$\mathcal{E}_{\varphi\mathrm{c}}^{\mathrm{E}} = \lim_{\rho\to 0}\int_{\Gamma^+(0)} q_s\phi_{,1} d\Gamma + \lim_{\rho\to 0}\int_{\Gamma^+} (-q_s\phi_{,1}) d\Gamma + \lim_{\rho\to 0}\int_{A_\rho}\int_0^t (E_{j,1}\mathrm{d}\,D_j - D_{j,1}\mathrm{d}\,E_j)\mathrm{d}A \tag{22}$$

3. Approximate evaluation of CED in arbitrary direction for linear problem and discussion based on some examples

Based on some assumptions, in this section, approximate expression of each mode contribution of CED is derived concretely for the case where linear singular solution is known. Using the obtained expressions, basic investigation about the effects of electric field and electrical boundary conditions on mixed mode fracture is then conducted.

3.1. Derivation of approximate expression of each mode contribution of CED in arbitrary direction

The first term of the right hand side in Eq. (22) becomes exactly 0 for an impermeable crack since surface charge q_s is 0 on the crack (notch) surface. Also for a real crack with a dielectric inclusion, the value of the term is supposed to be very small, compared to the second term. The value becomes larger as crack inclined angle to poling direction increases, but it is still expected not to have so much share compared to the second term. In addition, the area integral terms in Eqs. (20) and (22) seem to have negligible values in linear case when electromechanical proportional loads are applied. These facts could be confirmed by evaluating each term in Eqs. (20) and (22) with the help of finite element analysis.

Hereafter, consider a linear piezoelectric medium, with a crack arbitrarily oriented with respect to the poling direction, subjected to proportionally applied electromechanical loads, shown in Fig. 3. At least in this case, it can be said, through the results of finite element analysis, that neglecting the terms mentioned above does not cause a significant error in the accuracy. The details will be discussed in our following paper. Taking

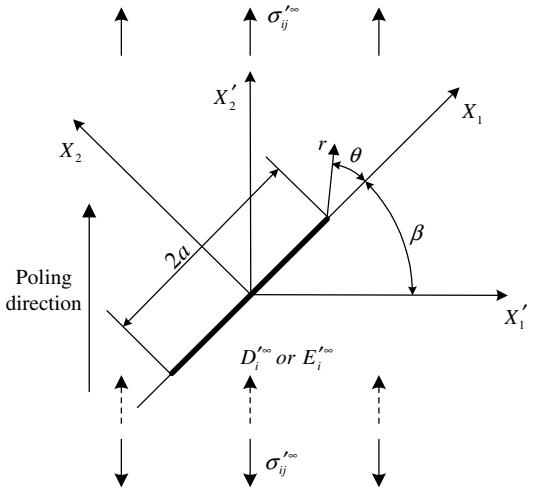

Fig. 3. An arbitrarily oriented crack subjected to electromechanical loadings.

also the fact that $\mathcal{E}^{\mathrm{E}}_{\varphi}$ has the same value as $\mathcal{E}^{\mathrm{E}}_{\varphi\mathrm{c}}$ in linear problem into account, therefore, following approximated equations hold:

$$\mathcal{E}^{\mathrm{M}}_{\varphi} \approx \lim_{\rho\to 0}\int_{\Gamma^+}(-T_i u_{i,1})\mathrm{d}\Gamma \tag{23}$$

$$\mathcal{E}^{\mathrm{E}}_{\varphi} \approx \lim_{\rho\to 0}\int_{\Gamma^+}(-q_s \phi_{,1})\mathrm{d}\Gamma \tag{24}$$

And their each mode contributions are now given as

$$\mathcal{E}^{\mathrm{MI}}_{\varphi} \approx \lim_{\rho\to 0}\int_{\Gamma^+}(-T_2 u_{2,1})\mathrm{d}\Gamma \tag{25}$$

$$\mathcal{E}^{\mathrm{MII}}_{\varphi} \approx \lim_{\rho\to 0}\int_{\Gamma^+}(-T_1 u_{1,1})\mathrm{d}\Gamma \tag{26}$$

$$\mathcal{E}^{\mathrm{EI}}_{\varphi} \approx \lim_{\rho\to 0}\int_{\Gamma^+}(-q_s \phi_{,1})\mathrm{d}\Gamma \tag{27}$$

It should be noted that mode II contribution of $\mathcal{E}^{\mathrm{E}}_{\varphi}$ does not exist essentially from the electrical nature, that is,

$$\mathcal{E}^{\mathrm{E}}_{\varphi} = \mathcal{E}^{\mathrm{EI}}_{\varphi}, \quad \mathcal{E}^{\mathrm{EII}}_{\varphi} = 0 \tag{28}$$

Thereby the mode separation of $\mathcal{E}^{\mathrm{E}}_{\varphi}$ in Eq. (3) is not so meaningful. However, it goes without saying that the relation as

$$\mathcal{E}^{\alpha}_{\varphi} = \mathcal{E}_{\varphi}{}^{\mathrm{M}\alpha} + \mathcal{E}^{\mathrm{E}\alpha}_{\varphi} \tag{29}$$

holds in general.

Now, let us think about Eqs. (25)–(27) further. In Fig. 1, let Γ^- be the path which encloses $\Gamma^-(0)$ and corresponds to Γ^+ when the rotation angle of x_1 and x_2 axes is φ'. Let $\sigma^{\mathrm{A(n)}}_{22}$ and $\sigma^{\mathrm{B(n)}}_{22}$ be the normal stress and shearing stress, respectively, that are zero on Γ^- and actually generate on Γ^+ and let $u^{\mathrm{A(n)}}_{2,1}$ and $u^{\mathrm{B(n)}}_{1,1}$ be the components of displacement gradient related to mode I and mode II deformations, respectively, that actually generates on $\Gamma^- + \Gamma^+$. Moreover, let $D^{\mathrm{A(n)}}_2$ and $\phi^{\mathrm{A(n)}}_{,1}$ be the electric displacement that is zero on Γ^- and actually generates on Γ^+ and the gradient of electric potential that actually generates on $\Gamma^- + \Gamma^+$, respectively. Considering the fact that $T_i = \sigma_{ij}n_j$, $q_s = -D_i n_i$ and $n_2\mathrm{d}\Gamma = -\mathrm{d}x_1$, Eqs. (25)–(27) can be expressed as

$$\mathcal{E}_{\varphi}^{\mathrm{MI}} \approx \lim_{\rho\to 0}\int_{\Gamma^+}(-T_2 u_{2,1})\mathrm{d}\Gamma = \lim_{\rho\to 0}\int_{\Gamma^-+\Gamma^+}\sigma_{22}^{\mathrm{A(n)}}u_{2,1}^{\mathrm{A(n)}}\mathrm{d}x_1 \tag{30}$$

$$\mathcal{E}_{\varphi}^{\mathrm{MII}} \approx \lim_{\rho\to 0}\int_{\Gamma^+}(-T_1 u_{1,1})\mathrm{d}\Gamma = \lim_{\rho\to 0}\int_{\Gamma^-+\Gamma^+}\sigma_{12}^{\mathrm{B(n)}}u_{1,1}^{\mathrm{B(n)}}\mathrm{d}x_1 \tag{31}$$

$$\mathcal{E}_{\varphi}^{\mathrm{EI}} \approx \lim_{\rho\to 0}\int_{\Gamma^+}(-q_s\phi_{,1})\mathrm{d}\Gamma = -\lim_{\rho\to 0}\int_{\Gamma^-+\Gamma^+}D_2^{\mathrm{A(n)}}\phi_{,1}^{\mathrm{A(n)}}\mathrm{d}x_1 \tag{32}$$

Now, consider, in Fig. 3, a crack when $\rho = 0$. For this crack, Xu and Rajapakse (2001) gave analytical singular solutions under some representative crack surface boundary conditions as shown in Appendix A. In the coordinate system (x_1, x_2, x_3) rotated by angle φ with respect to X_1 axis, singular field solutions of Eqs. (A.1)–(A.4) are expressed by using polar coordinate (r, θ) depicted in Fig. 4 as

$$\begin{pmatrix}\sigma_{11}\\ \sigma_{22}\\ \sigma_{12}\end{pmatrix} = \frac{1}{\sqrt{2r}}\mathrm{Re}\sum_{k=1}^{3}\begin{Bmatrix}(\sin\varphi-\mu_k\cos\varphi)^2\\ (\cos\varphi+\mu_k\sin\varphi)^2\\ (\cos\varphi+\mu_k\sin\varphi)(\sin\varphi-\mu_k\cos\varphi)\end{Bmatrix}\frac{h_k}{\sqrt{\cos\theta+\mu_k\sin\theta}} \tag{33}$$

$$\begin{pmatrix}D_1\\ D_2\end{pmatrix} = -\frac{1}{\sqrt{2r}}\mathrm{Re}\sum_{k=1}^{3}\begin{Bmatrix}\lambda_k(\sin\varphi-\mu_k\cos\varphi)\\ \lambda_k(\cos\varphi+\mu_k\sin\varphi)\end{Bmatrix}\frac{h_k}{\sqrt{\cos\theta+\mu_k\sin\theta}} \tag{34}$$

$$\begin{pmatrix}E_1\\ E_2\end{pmatrix} = \frac{1}{\sqrt{2r}}\mathrm{Re}\sum_{k=1}^{3}\begin{Bmatrix}r_k\cos\varphi-s_k\sin\varphi\\ -r_k\sin\varphi-s_k\cos\varphi\end{Bmatrix}\frac{h_k}{\sqrt{\cos\theta+\mu_k\sin\theta}} \tag{35}$$

$$\begin{pmatrix}u_1\\ u_2\\ \phi\end{pmatrix} = \sqrt{2r}\mathrm{Re}\sum_{k=1}^{3}\begin{Bmatrix}(p_k\cos\varphi+q_k\sin\varphi)\\ (-p_k\sin\varphi+q_k\cos\varphi)\\ -r_k\end{Bmatrix}h_k\sqrt{\cos\theta+\mu_k\sin\theta} \tag{36}$$

where μ_k, λ_k, r_k, s_k, p_k and q_k are the constants determined from material properties and their specific information are provided in Appendix A.

Now, in the rotated coordinate (x_1, x_2, x_3) by the amount of φ, consider a point P at an arbitrary θ and its symmetric point with respect to the x_1–x_3 plane P' as shown in Fig. 4. Here, symmetric point P' is, if $\varphi \geqslant 0^\circ$ as shown in figure, at $2\varphi-\theta$ when $2\varphi-180^\circ \leqslant \theta \leqslant 180^\circ$ and at $2\varphi-\theta-360^\circ$ when $-180^\circ \leqslant \theta \leqslant 2\varphi-180^\circ$, respectively, and, if $\varphi < 0^\circ$, it is at $2\varphi-\theta$ when $-180^\circ \leqslant \theta \leqslant 2\varphi+180^\circ$ and at $2\varphi-\theta+360^\circ$ when $2\varphi+180^\circ \leqslant \theta \leqslant 180^\circ$, respectively. Next, define the quantities given by

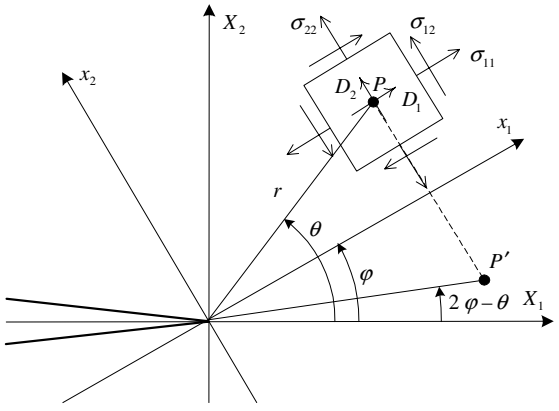

Fig. 4. Stresses and electric displacement in the coordinate system rotated by angle φ.

$$
\begin{aligned}
\sigma_{22}^{\mathrm{A}}(\theta) &= \{\sigma_{22}(\theta) + \sigma_{22}(2\varphi - \theta)\}/2 \\
\sigma_{22}^{\mathrm{B}}(\theta) &= \{\sigma_{22}(\theta) - \sigma_{22}(2\varphi - \theta)\}/2 \\
\sigma_{12}^{\mathrm{A}}(\theta) &= \{\sigma_{12}(\theta) - \sigma_{12}(2\varphi - \theta)\}/2 \\
\sigma_{12}^{\mathrm{B}}(\theta) &= \{\sigma_{12}(\theta) + \sigma_{12}(2\varphi - \theta)\}/2 \\
D_2^{\mathrm{A}}(\theta) &= \{D_2(\theta) + D_2(2\varphi - \theta)\}/2 \\
D_2^{\mathrm{B}}(\theta) &= \{D_2(\theta) - D_2(2\varphi - \theta)\}/2 \\
u_{2,1}^{\mathrm{A}}(\theta) &= \{u_{2,1}(\theta) - u_{2,1}(2\varphi - \theta)\}/2 \\
u_{2,1}^{\mathrm{B}}(\theta) &= \{u_{2,1}(\theta) + u_{2,1}(2\varphi - \theta)\}/2 \\
u_{1,1}^{\mathrm{A}}(\theta) &= \{u_{1,1}(\theta) + u_{1,1}(2\varphi - \theta)\}/2 \\
u_{1,1}^{\mathrm{B}}(\theta) &= \{u_{1,1}(\theta) - u_{1,1}(2\varphi - \theta)\}/2 \\
\phi_{,1}^{\mathrm{A}}(\theta) &= \{\phi_{,1}(\theta) - \phi_{,1}(2\varphi - \theta)\}/2 \\
\phi_{,1}^{\mathrm{B}}(\theta) &= \{\phi_{,1}(\theta) + \phi_{,1}(2\varphi - \theta)\}/2
\end{aligned}
\tag{37}
$$

for when $\varphi \geqslant 0^\circ$ and $2\varphi - 180^\circ \leqslant \theta \leqslant 180^\circ$ or when $\varphi < 0^\circ$ and $-180^\circ \leqslant \theta \leqslant 2\varphi + 180^\circ$, and

$$
\begin{aligned}
\sigma_{22}^{\mathrm{A}}(\theta) &= \{\sigma_{22}(\theta) - \sigma_{22}(2\varphi - \theta \mp 360^\circ)\}/2 \\
\sigma_{22}^{\mathrm{B}}(\theta) &= \{\sigma_{22}(\theta) + \sigma_{22}(2\varphi - \theta \mp 360^\circ)\}/2 \\
\sigma_{12}^{\mathrm{A}}(\theta) &= \{\sigma_{12}(\theta) + \sigma_{12}(2\varphi - \theta \mp 360^\circ)\}/2 \\
\sigma_{12}^{\mathrm{B}}(\theta) &= \{\sigma_{12}(\theta) - \sigma_{12}(2\varphi - \theta \mp 360^\circ)\}/2 \\
D_2^{\mathrm{A}}(\theta) &= \{D_2(\theta) - D_2(2\varphi - \theta \mp 360^\circ)\}/2 \\
D_2^{\mathrm{B}}(\theta) &= \{D_2(\theta) + D_2(2\varphi - \theta \mp 360^\circ)\}/2 \\
u_{2,1}^{\mathrm{A}}(\theta) &= \{u_{2,1}(\theta) + u_{2,1}(2\varphi - \theta \mp 360^\circ)\}/2 \\
u_{2,1}^{\mathrm{B}}(\theta) &= \{u_{2,1}(\theta) - u_{2,1}(2\varphi - \theta \mp 360^\circ)\}/2 \\
u_{1,1}^{\mathrm{A}}(\theta) &= \{u_{1,1}(\theta) - u_{1,1}(2\varphi - \theta \mp 360^\circ)\}/2 \\
u_{1,1}^{\mathrm{B}}(\theta) &= \{u_{1,1}(\theta) + u_{1,1}(2\varphi - \theta \mp 360^\circ)\}/2 \\
\phi_{,1}^{\mathrm{A}}(\theta) &= \{\phi_{,1}(\theta) + \phi_{,1}(2\varphi - \theta \mp 360^\circ)\}/2 \\
\phi_{,1}^{\mathrm{B}}(\theta) &= \{\phi_{,1}(\theta) - \phi_{,1}(2\varphi - \theta \mp 360^\circ)\}/2
\end{aligned}
\tag{38}
$$

for when $\varphi \geqslant 0^\circ$ and $-180^\circ \leqslant \theta \leqslant 2\varphi - 180^\circ$ (apply '$-$' sign in Eq. (38)) or when $\varphi < 0^\circ$ and $2\varphi + 180^\circ \leqslant \theta \leqslant 180^\circ$ (apply '$+$' sign in Eq. (38)). It is easily seen that, in general, when $\varphi \geqslant 0^\circ$, the quantities with superscript A are symmetric with respect to the x_1–x_3 plane for $2\varphi - 180^\circ \leqslant \theta \leqslant 180^\circ$ and anti-symmetric for $-180^\circ \leqslant \theta \leqslant 2\varphi - 180^\circ$, and, when $\varphi < 0^\circ$, symmetric for $-180^\circ \leqslant \theta \leqslant 2\varphi + 180^\circ$ and anti-symmetric for $2\varphi + 180^\circ \leqslant \theta \leqslant 180^\circ$. The quantities with superscript B are, on the contrary, anti-symmetric for $2\varphi - 180^\circ \leqslant \theta \leqslant 180^\circ$ and symmetric for$-180^\circ \leqslant \theta \leqslant 2\varphi - 180^\circ$ when $\varphi \geqslant 0^\circ$, and anti-symmetric for $-180^\circ \leqslant \theta \leqslant 2\varphi + 180^\circ$ and symmetric for $2\varphi + 180^\circ \leqslant \theta \leqslant 180^\circ$ when $\varphi < 0^\circ$. The sum of the quantities at θ with A and B coincides with the original quantity at θ and it is naturally considered that symmetric and anti-symmetric quantities are related to mode I and mode II deformations, respectively.

Here, let us apply Eqs. (33)–(36) to Eqs. (37) and (38) and let, for instance, $\sigma_{22}^{\mathrm{A}*}$ be the distribution of stress along x_1 axis obtained from $\sigma_{22}^{A}(\varphi)$ and $\sigma_{22}^{A}(\varphi - 180^\circ)$. Moreover, let $u_{2,1}^{\mathrm{A}_+^*}$ be the distribution of the displacement gradient along x_1 axis obtained from $u_{2,1}^{A}(\varphi^+)$ and $u_{2,1}((\varphi - 180^\circ)^+)$, and $u_{2,1}^{\mathrm{A}_-^*}$ be that obtained from $u_{2,1}^{A}(\varphi^-)$ and $u_{2,1}^{A}((\varphi - 180^\circ)^-)$. Symbols+ and − are attached to discriminate between the quantities on x_1–x_3 plane of positive $x_2$side and on x_1–x_3 plane of negative x_2 side. Then, introducing Heaviside function H, the following equations for and $u_{2,1}^{A_+^*} - u_{2,1}^{A_-^*}$ are derived.

$$\sigma_{22}^{A^*} = \frac{H(x_1)}{\sqrt{2x_1}} \mathrm{Re} \sum_{k=1}^{3} h_k (\cos\varphi + \mu_k \sin\varphi)^{3/2} \tag{39}$$

$$u_{2,1}^{A_+^*} - u_{2,1}^{A_-^*} = -\frac{2H(-x_1)}{\sqrt{2(-x_1)}} \mathrm{Im} \sum_{k=1}^{3} h_k (p_k \sin\varphi - q_k \cos\varphi)(\cos\varphi + \mu_k \sin\varphi)^{1/2} \tag{40}$$

The distributions of Eqs. (39) and (40) are shown schematically in Fig. 5(a) and (b), respectively, for reference. Letting $\sigma_{12}^{B^*}$ and $D_2^{A^*}$ be the quantities defined in the same way as $\sigma_{22}^{A^*}$ and, moreover, $(u_{1,1}^{B_+^*}, u_{1,1}^{B_-^*})$ and $(\phi_{,1}^{A_+^*}, \phi_{,1}^{A_-^*})$ be the quantities defined in the same way as $(u_{2,1}^{A_+^*}, u_{2,1}^{B_-^*})$, also the following equations are obtained.

$$\sigma_{12}^{B^*} = \frac{H(x_1)}{\sqrt{2x_1}} \mathrm{Re} \sum_{k=1}^{3} h_k (\cos\varphi + \mu_k \sin\varphi)^{1/2} (\sin\varphi - \mu_k \cos\varphi) \tag{41}$$

$$u_{1,1}^{B_+^*} - u_{1,1}^{B_-^*} = \frac{2H(-x_1)}{\sqrt{2(-x_1)}} \mathrm{Im} \sum_{k=1}^{3} h_k (p_k \cos\varphi + q_k \sin\varphi)(\cos\varphi + \mu_k \sin\varphi)^{1/2} \tag{42}$$

$$D_2^{A^*} = -\frac{H(x_1)}{\sqrt{2x_1}} \mathrm{Re} \sum_{k=1}^{3} h_k \lambda_k (\cos\varphi + \mu_k \sin\varphi)^{1/2} \tag{43}$$

$$\phi_{,1}^{A_+^*} - \phi_{,1}^{A_-^*} = -\frac{2H(-x_1)}{\sqrt{2(-x_1)}} \mathrm{Im} \sum_{k=1}^{3} h_k r_k (\cos\varphi + \mu_k \sin\varphi)^{1/2} \tag{44}$$

Now, consider again $(\sigma_{22}^{A(n)}, \sigma_{12}^{B(n)}, D_2^{A(n)})$ and $(u_{2,1}^{A(n)}, u_{1,1}^{B(n)}, \phi_{,1}^{A(n)})$ in Eqs. (30)–(32). It is easily seen that $(\sigma_{22}^{A(n)}, \sigma_{12}^{B(n)}, D_2^{A(n)})$ coincides with $(\sigma_{22}^{A^*}, \sigma_{12}^{B^*}, D_2^{A^*})$ and $(u_{2,1}^{A(n)}, u_{1,1}^{B(n)}, \phi_{,1}^{A(n)})$ does with, in the side of positive x_2, $(u_{2,1}^{A_+^*}, u_{1,1}^{B_+^*}, \phi_{,1}^{A_+^*})$ and, in the side of negative x_2, $(u_{2,1}^{A_-^*}, u_{1,1}^{B_-^*}, \phi_{,1}^{A_-^*})$ in the limit when $\rho \to 0$. Accordingly, taking the relation

$$\lim_{\eta \to 0} \int_{-\eta}^{\eta} \frac{H(x_1)}{\sqrt{x_1}} \frac{H(-x_1)}{\sqrt{-x_1}} dx_1 = \frac{\pi}{2} \tag{45}$$

into consideration, the following equations for $\mathcal{E}_\varphi^{MI}$, $\mathcal{E}_\varphi^{MII}$ and $\mathcal{E}_\varphi^{EI}$ in Eqs. (30)–(32) are obtained.

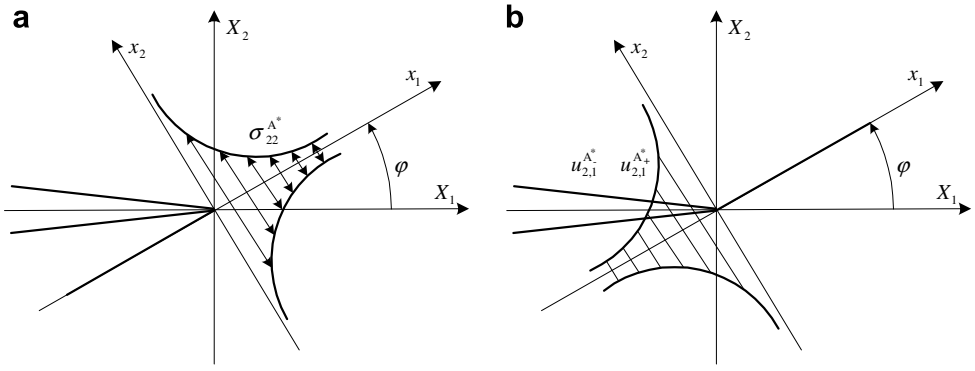

Fig. 5. Schematic distributions of stress and difference of displacement gradients between upper and lower planes of x_1–x_3 plane corresponding to Eqs. (39) and (40).

$$\mathcal{E}_{\varphi}^{\mathrm{MI}} \approx \lim_{\Delta b\to 0}\lim_{\rho\to 0}\int_{\Gamma^-+\Gamma^+}\sigma_{22}^{\mathrm{A(n)}}u_{2,1}^{\mathrm{A(n)}}\mathrm{d}x_1 = -\lim_{\eta\to 0}\int_{-\eta}^{\eta}\sigma_{22}^{\mathrm{A}^*}(u_{2,1}^{\mathrm{A}_+^*}-u_{2,1}^{\mathrm{A}_-^*})\mathrm{d}x_1$$
$$= \frac{\pi}{2}\mathrm{Re}\sum_{k=1}^{3}h_k(\cos\varphi+\mu_k\sin\varphi)^{3/2}\mathrm{Im}\sum_{k=1}^{3}h_k(p_k\sin\varphi-q_k\cos\varphi)(\cos\varphi+\mu_k\sin\varphi)^{1/2} \tag{46}$$

$$\mathcal{E}_{\varphi}^{\mathrm{MII}} \approx \lim_{\Delta b\to 0}\lim_{\rho\to 0}\int_{\Gamma^-+\Gamma^+}\sigma_{12}^{\mathrm{B(n)}}u_{1,1}^{\mathrm{B(n)}}\mathrm{d}x_1 = -\lim_{\eta\to 0}\int_{-\eta}^{\eta}\sigma_{12}^{\mathrm{B}^*}(u_{2,1}^{\mathrm{B}_+^*}-u_{2,1}^{\mathrm{B}_-^*})\mathrm{d}x_1$$
$$= -\frac{\pi}{2}\mathrm{Re}\sum_{k=1}^{3}h_k(\sin\varphi-\mu\cos\varphi)(\cos\varphi+\mu_k\sin\varphi)^{1/2}\mathrm{Im}\sum_{k=1}^{3}h_k(p_k\cos\varphi+q_k\sin\varphi)$$
$$\times(\cos\varphi+\mu_k\sin\varphi)^{1/2} \tag{47}$$

$$\mathcal{E}_{\varphi}^{\mathrm{EI}} \approx -\lim_{\Delta b\to 0}\lim_{\rho\to 0}\int_{\Gamma^-+\Gamma^+}D_2^{\mathrm{A(n)}}\phi_{,1}^{\mathrm{A(n)}}\mathrm{d}x_1 = \lim_{\eta\to 0}\int_{-\eta}^{\eta}D_2^{\mathrm{A}^*}(\phi_{,1}^{\mathrm{A}_+^*}-\phi_{,1}^{\mathrm{A}_-^*})\mathrm{d}x_1$$
$$= \frac{\pi}{2}\mathrm{Re}\sum_{k=1}^{3}h_k\lambda_k(\cos\varphi+\mu_k\sin\varphi)^{1/2}\mathrm{Im}\sum_{k=1}^{3}h_kr_k(\cos\varphi+\mu_k\sin\varphi)^{1/2} \tag{48}$$

Here, $(\eta(>0),0)$ is an arbitrary point on x_1 axis. Since the contribution of $\sigma_{22}^{\mathrm{A(n)}}u_{2,1}^{\mathrm{A(n)}}$ (or $\sigma_{22}^{A^*}(u_{2,1}^{A_+^*}-u_{2,1}^{\mathrm{A}_-^*})$), for example, to the integration value appears just at singular crack tip point, $\mathcal{E}_{\varphi}^{\mathrm{MI}}$ in Eq. (30) can be evaluated as the limit when $\Delta b\to 0$ (or $\eta\to 0$) in Eq. (46), and the same goes also for $\mathcal{E}_{\varphi}^{\mathrm{MII}}$ and $\mathcal{E}_{\varphi}^{\mathrm{EI}}$. Using the relation of Eq. (29) and Eqs. (46), (47), one can easily have the expressions of $\mathcal{E}_{\varphi}^{\alpha}$. Note that obtained equations are rightly identical to the results for self-similar crack, if both crack inclined angle β and φ are equal to zero (Nam and Watanabe, 2007, 2008).

3.2. Numerical examples and discussion

The equations to evaluate each mode contribution of CED in arbitrary direction, although they are approximate ones and are available under proportionally applied electromechanical load, were obtained in previous subsection for the problem shown in Fig. 3. The characteristics of CED and its each mode contribution, whatever the fracture parameter is, will give us useful information to consider mixed mode fracture of piezoelectrics. So, their some fundamental characteristics obtained from Eqs. (46) and (48) are investigated here. Mode I type fracture occurs usually in brittle materials like ceramics. Accordingly, $\mathcal{E}_{\varphi}^{\mathrm{MI}}$, that is the work mechanically done to open the plane our attention is paid to, is considered to be the most promising parameter and, if so, it is quite natural to think that crack extension occurs in the direction where $\mathcal{E}_{\varphi}^{\mathrm{MI}}$ takes the maximum value when its maximum value reaches some critical value. And, the applicability of this way of thinking was demonstrated for the case of mode I crack where $\mathcal{E}_{\varphi}^{\mathrm{MI}}$ takes the maximum value and $\mathcal{E}_{\varphi}^{\mathrm{MII}}=0$ in the direction of $\varphi=0^\circ$ (Nam et al., 2007). Considering these, the investigations are conducted especially focusing on $\mathcal{E}_{\varphi}^{\mathrm{MI}}$, although what parameter is the most favorable is still an issue to be discussed further.

The problem dealt with is as was shown in Fig. 3 and PZT-4 was supposed as the material, of which the material properties are shown in Table 1. Dielectric inclusion inside the crack was assumed to be air with dielectric constant $\kappa_0=8.85\times10^{-12}\ \mathrm{C^2/Nm^2}$. Applied stress was kept at $\sigma_{22}'^{\infty}=1\ \mathrm{MPa}$ $(\sigma_{11}'^{\infty}=\sigma_{12}'^{\infty}=0)$ through the study.

The effect of electric field on each parameter in case of $\beta=0^\circ$ was investigated first under impermeable boundary condition. Figs. 6–8 show the variations of CED and its derivatives in arbitrary direction under relatively weak electric field, i.e., $E_2'^{\infty}=0\ \mathrm{V/m}$, $E_2'^{\infty}=2\times10^4\ \mathrm{V/m}$ and $E_2'^{\infty}=-2\times10^4\ \mathrm{V/m}$ ($E_1'^{\infty}=0$ through

Table 1
Material property for PZT-4 piezoelectric ceramics

Elastic constants (10^{10} N/m^2)					Piezoelectric constants (C/m^2)			Dielectric constants (10^{-9} C/Vm)	
c_{11}	c_{12}	c_{13}	c_{33}	c_{44}	e_{31}	e_{33}	e_{15}	κ_{11}	κ_{33}
13.9	7.78	7.43	11.3	2.56	−6.98	13.84	13.44	6.0	5.47

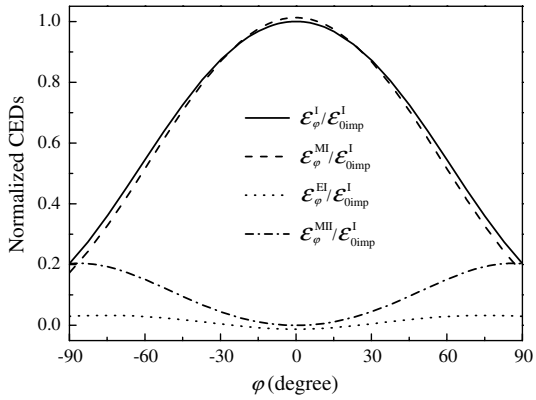

Fig. 6. Variations of normalized CED and its derivatives in arbitrary direction for a crack of $\beta = 0^\circ$ subjected to only mechanical loading under impermeable boundary condition ($\sigma_{22}'^{\infty} = 1$ MPa and $E_2'^{\infty} = 0$ V/m).

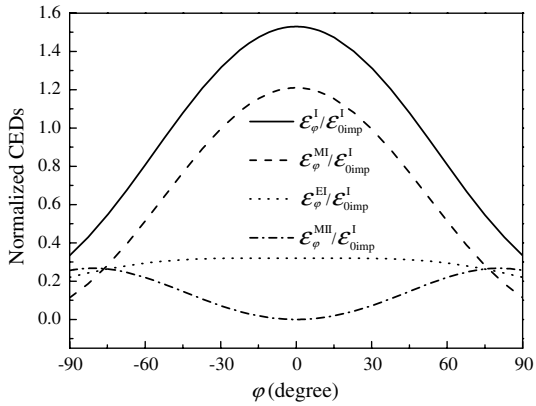

Fig. 7. Variations of normalized CED and its derivatives in arbitrary direction for a crack of $\beta = 0^\circ$ subjected to mechanical loading and positive electric field under impermeable boundary condition ($\sigma_{22}'^{\infty} = 1$ MPa and $E_2'^{\infty} = 2 \times 10^4$ V/m).

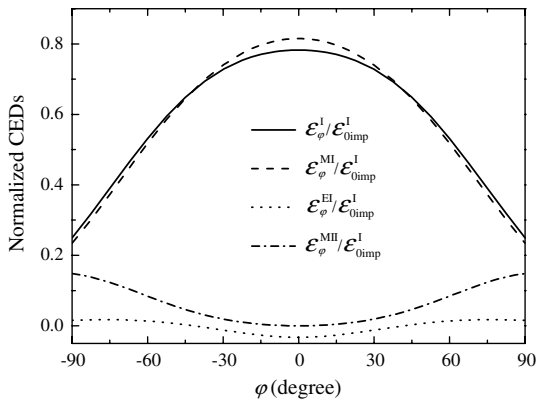

Fig. 8. Variation of normalized CED and its derivatives in arbitrary direction for a crack of $\beta = 0^\circ$ subjected to mechanical loading and negative electric field under impermeable boundary condition ($\sigma_{22}'^{\infty} = 1$ MPa and $E_2'^{\infty} = -2 \times 10^4$ V/m).

the study), respectively. Each parameter was normalized by $\mathcal{E}_{0\mathrm{imp}}^{\mathrm{I}}$, which means mode I contribution of CED in self-similar direction ($\varphi = 0^\circ$) in the absence of electric field under impermeable condition. The figures show that all the parameters, especially mode I contributions, are greatly influenced by applied electric field. $\mathcal{E}_\varphi^{\mathrm{I}}$ and

$\mathcal{E}_{\varphi}^{\mathrm{MI}}$ have the greatest at $\varphi = 0°$, while $\mathcal{E}_{\varphi}^{\mathrm{MII}}$ has the greatest at about $\varphi = \pm 90°$. With all that, variation of $\mathcal{E}_{\varphi}^{\mathrm{EI}}$ with φ is slight. And $\mathcal{E}_{\varphi}^{\mathrm{I}}$ and $\mathcal{E}_{\varphi}^{\mathrm{MI}}$ increase in case of positive electric field and decrease in case of negative electric field. The results by $\mathcal{E}_{\varphi}^{\mathrm{I}}$ and $\mathcal{E}_{\varphi}^{\mathrm{MI}}$ have a tendency to be consistent with the experimental result by Park and Sun (1995), which indicated that positive electric field could enhance crack extension and negative electric field could retard it.

Influence of electric boundary condition mentioned in Appendix A is then investigated. Fig. 9 shows, for an instance, the variations of $\mathcal{E}_{\varphi}^{\mathrm{MI}}$ when $E_2'^{\infty} = \pm 2 \times 10^4$ V/m under different electrical boundary conditions. Applied electric field has little effect on the parameter under exact or Hao and Shen type boundary condition, contrary to under impermeable boundary condition. Substituting D_2^0 in Eq. (A.16) into Eq. (A.7), we can easily see that electric displacement applied at far field D_2^{∞} is eliminated. This is why remote electric loading has no influence on the parameter under exact boundary condition. There exists the difference between positive and negative applied electric fields under Hao and Shen type boundary condition, but it is not clear in Fig. 9 simply because the electric loading is relatively weak. Other parameters except $\mathcal{E}_{\varphi}^{\mathrm{MI}}$ had the same tendency with regard to the effect of electrical boundary condition.

Fig. 10 shows the variation of $\mathcal{E}_{\varphi}^{\mathrm{MI}}$ under Hao and Shen type boundary condition when applied electric field is relatively strong ranging from -6×10^5 to 6×10^5 V/m. $\mathcal{E}_{\varphi}^{\mathrm{MI}}$ increases continuously as applied electric field increases from negative ones to positive ones, meaning that the increment of electric field enhances crack extension. We can also see that the direction in which $\mathcal{E}_{\varphi}^{\mathrm{MI}}$ has the greatest value remains unchanged as $\varphi = 0°$ for any electric loading.

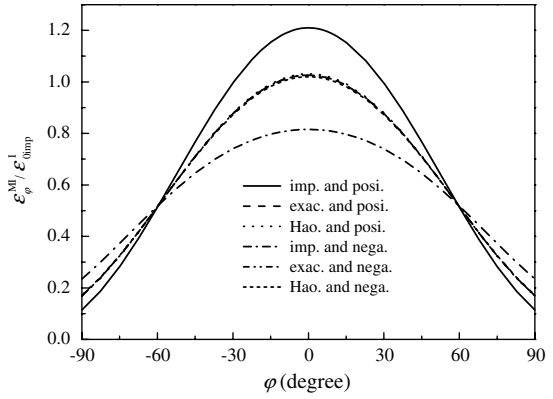

Fig. 9. The effect of electric boundary conditions on normalized $\mathcal{E}_{\varphi}^{\mathrm{MI}}$ for a crack of $\beta = 0°$ when $E_2'^{\infty} = \pm 2 \times 10^4$ V/m ($\sigma_{22}'^{\infty} = 1$ MPa).

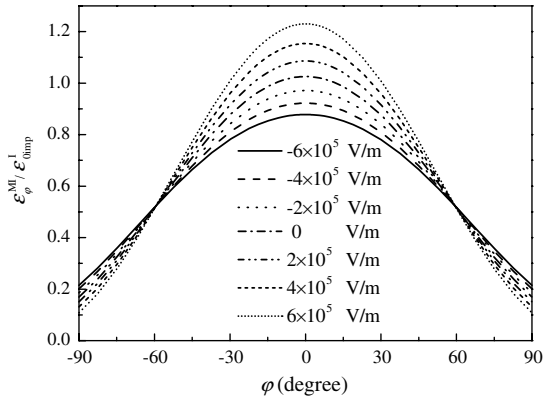

Fig. 10. Variation of normalized $\mathcal{E}_{\varphi}^{\mathrm{MI}}$ for a crack of $\beta = 0°$ under Hoa and Shen type boundary condition when applied electric field is relatively strong ($\sigma_{22}'^{\infty} = 1$ MPa).

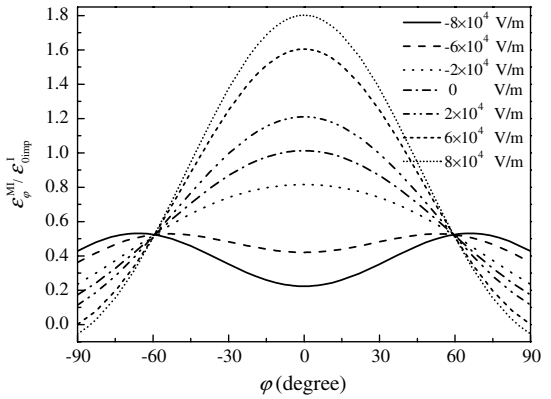

Fig. 11. Variation of normalized $\mathcal{E}_\varphi^{MI}$ for a crack of $\beta = 0^\circ$ under impermeable boundary condition when applied electric field is relatively weak ($\sigma_{22}'^{\infty} = 1$ MPa).

Fig. 11 shows the variation of $\mathcal{E}_\varphi^{MI}$ under impermeable boundary condition when applied electric field changes from -8×10^4 to 8×10^4 V/m. In contrast to under Hao and Shen type boundary condition, the effect of electric field on the parameter is notable even at a weak level of electric field. It should be noted that, with increasing negative electric field, the greatest value of $\mathcal{E}_\varphi^{MI}$ is not at $\varphi = 0^\circ$ any more and it is nearly at $\varphi = \pm 60^\circ$ when applied electric field is below -6×10^4 V/m. This fact is qualitatively consistent with the observation of McHenry and Koepke (1983), as introduced in Introduction: crack propagation could be deviated from its original direction under a strong electric field.

It is likely that we need to touch on electric boundary conditions here. Exact boundary condition has been regarded as the best one for describing this dielectric inclusion problem. However, it seems not to be practical for explaining the effect of electric field, as was shown in Fig. 9. This is because a crack of $\rho = 0$ is employed as the model of a crack. An ideally sharp crack has no width, different from an actual crack with small but finite width, and this must be one of the demerits of usually employed ideally sharp crack model for this dielectric inclusion problem. Even though Hao and Shen type boundary condition may be one of the approximated conditions to overcome the demerit of exact boundary condition, it expresses the effect of electric field well as shown above. Impermeable boundary condition is also qualitatively admissible if one considers the safety of the design, since the parameters are always overestimated under the condition. In addition, it is well known that the values under exact boundary condition approach those under the impermeable crack when the ratio of the width to crack length, i.e. ρ/a in Fig. 1, is larger than 10^{-2} (Sosa and Khutoryansky, 1996; Zhang et al., 1998).

Next, Figs. 12 and 13 show the variation of each parameter under impermeable boundary condition when $\beta = 30^\circ$ and $\beta = 60^\circ$, respectively. Applied electric field was $E_2'^{\infty} = -2 \times 10^4$ V/m. Compared with the case of $\beta = 0^\circ$ of Fig. 8, the absolute values of angle φ, at which $\mathcal{E}_\varphi^{I}$ and $\mathcal{E}_\varphi^{MI}$ are the greatest, become larger as β increases. Moreover, the ratio of mode II contribution to mode I contribution for mechanical CED ($\mathcal{E}_\varphi^{MII}/\mathcal{E}_\varphi^{MI}$) at their maximum values also increases gradually with increasing β.

For a crack of $\beta = 30^\circ$ or $\beta = 60^\circ$, each parameter, although the figures are not shown here, had the same tendency in the effect of electric boundary condition as that of $\beta = 0^\circ$ in Fig. 9. Figs. 14 and 15 show, as corresponding cases of Fig. 11 when $\beta = 0^\circ$, the influences of electric field on $\mathcal{E}_\varphi^{MI}$ under Hao and Shen type boundary condition for $\beta = 30^\circ$ and $\beta = 60^\circ$, respectively. As β increases, the effect of electric field on the parameter decreased, and we could confirm that the effect finally disappears when $\beta = 90^\circ$.

Figs. 16 and 17 show the effect of electric filed on $\mathcal{E}_\varphi^{MI}$ under impermeable boundary condition when $\beta = 30^\circ$ and $\beta = 60^\circ$, respectively. The direction where $\mathcal{E}_\varphi^{MI}$ takes the greatest value, slightly changed even under positive applied electric fields as well as under negative ones in spite of low level of applied electric fields. For the impermeable crack, relationship between applied electric field and the direction is summarized in Fig. 18 from the results of Figs. 12, 17 and 18. It shows that with increasing positive electric fields the direction where $\mathcal{E}_\varphi^{MI}$

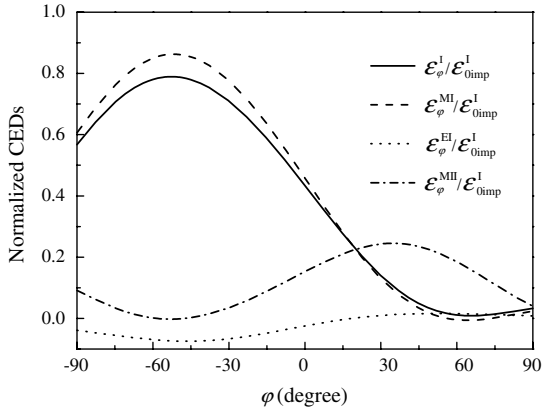

Fig. 12. Variations of normalized CED and its derivatives in arbitrary direction for an inclined crack of $\beta = 30^\circ$ subjected to mechanical loading and negative electric field under impermeable boundary condition ($\sigma_{22}'^{\infty} = 1$ MPa and $E_2'^{\infty} = -2 \times 10^4$ V/m).

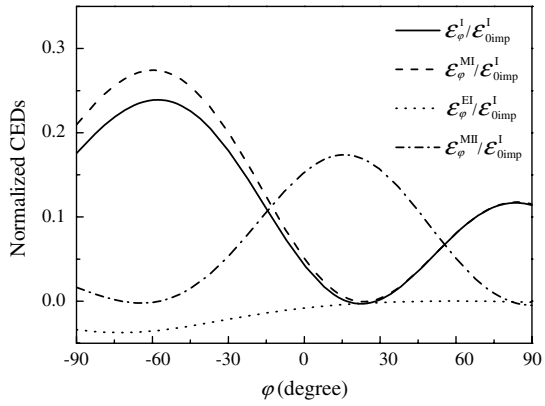

Fig. 13. Variations of normalized CED and its derivatives in arbitrary direction for an inclined crack of $\beta = 60^\circ$ subjected to mechanical loading and negative electric field under impermeable boundary condition ($\sigma_{22}'^{\infty} = 1$ MPa and $E_2'^{\infty} = -2 \times 10^4$ V/m).

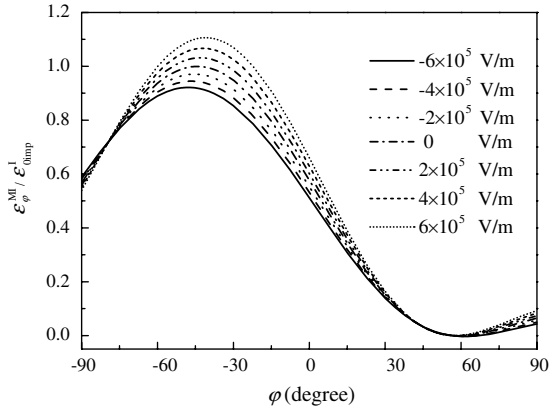

Fig. 14. Variation of normalized $\mathcal{E}_\varphi^{\mathrm{MI}}$ for a crack of $\beta = 30^\circ$ under Hoa and Shen type boundary condition when applied electric field is relatively strong ($\sigma_{22}'^{\infty} = 1$ MPa).

takes the greatest value remains unchanged in case of $\beta = 0^\circ$ and slightly decreases in cases of $\beta = 30^\circ$ and $\beta = 60^\circ$. In contrast, with increasing negative electric fields it sharply increases in all cases, especially in case of $\beta = 0^\circ$.

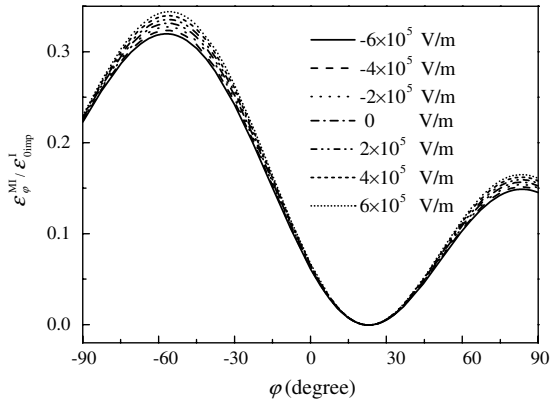

Fig. 15. Variation of normalized $\mathcal{E}_\varphi^{MI}$ for a crack of $\beta = 60^\circ$ under Hoa and Shen type boundary condition when applied electric field is relatively strong ($\sigma_{22}'^{\infty} = 1$ MPa).

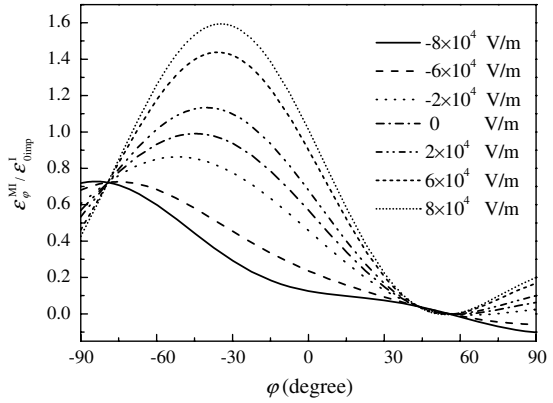

Fig. 16. Variation of normalized $\mathcal{E}_\varphi^{MI}$ for a crack of $\beta = 30^\circ$ under impermeable boundary condition when applied electric field is relatively weak ($\sigma_{22}'^{\infty} = 1$ MPa).

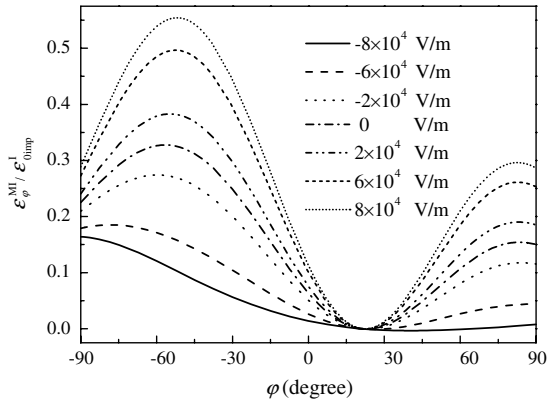

Fig. 17. Variation of normalized $\mathcal{E}_\varphi^{MI}$ for a crack of $\beta = 60^\circ$ under impermeable boundary condition when applied electric field is relatively weak ($\sigma_{22}'^{\infty} = 1$ MPa).

4. Conclusions

The concept of crack energy density for piezoelectric material was extended so as to be meaningful also in an arbitrary direction for the treatment of electromechanical mixed mode fracture, and it was shown that the CED in arbitrary direction is generally divided into mechanical mode I and mode II parts and electrical mode I part and

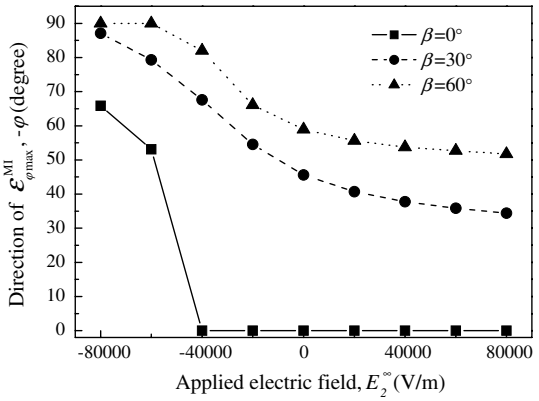

Fig. 18. Relationship between applied electric field and crack extension direction for impermeable crack ($\sigma'^{\infty}_{22} = 1$ MPa).

each of them has its own path independent expression. Based on path independent expressions, moreover, approximate equations of each quantity were obtained for a linear electromechanical crack problem and the effects of applied electric field and electric boundary condition on the CED and its derivatives were investigated. Especially, the results for mode I contribution of mechanical CED, $\mathcal{E}^{MI}_{\varphi}$, are summarized as follows:

1. Applied electric field influences more notably on $\mathcal{E}^{MI}_{\varphi}$ under impermeable boundary condition than under exact or Hao and Shen type boundary condition.
2. $\mathcal{E}^{MI}_{\varphi}$ under impermeable and Hao and Shen type boundary conditions shows qualitative agreement with existing experimental results on the effect of applied electric field. However,
3. $\mathcal{E}^{MI}_{\varphi}$ under exact boundary condition is not affected by applied electric field. This fact comes from the use of ideally sharp crack model and this is a demerit of ideally sharp crack model.
4. Crack propagation could be deviated from its self-similar direction under a strong negative electric field even when crack plane is perpendicular to poling direction.
5. The effect of electric field becomes smaller as crack plane inclines, and finally disappears when crack plane becomes parallel to poling direction.

Appendix A

Details of electromechanical singular solutions near a piezoelectric crack tip can be found in Xu and Rajapakse's work (2001) and the results used in this paper are summarized in the following. Consider an infinite piezoelectric plane polarized in the X'_2-direction and containing a dielectric crack oriented with respect to the poling direction by angle β, as shown in Fig. 3. Uniform electromechanical loadings σ'^{∞}_{ij} and D'^{∞}_{ij} (or E'^{∞}_{ij}) in (X'_1, X'_2) coordinate system are applied at far field. The solutions of singular field for this problem is given, using the polar coordinate system (r, θ), by

$$\begin{pmatrix}\sigma_{11}\\ \sigma_{22}\\ \sigma_{12}\end{pmatrix} = \frac{1}{\sqrt{2r}}\mathrm{Re}\sum_{k=1}^{3}\begin{Bmatrix}\mu_k^2\\ 1\\ -\mu_k\end{Bmatrix}\frac{h_k}{\sqrt{\cos\theta+\mu_k\sin\theta}} \tag{A.1}$$

$$\begin{pmatrix}D_1\\ D_2\end{pmatrix} = \frac{1}{\sqrt{2r}}\mathrm{Re}\sum_{k=1}^{3}\begin{Bmatrix}\lambda_k\mu_k\\ -\lambda_k\end{Bmatrix}\frac{h_k}{\sqrt{\cos\theta+\mu_k\sin\theta}} \tag{A.2}$$

$$\begin{pmatrix}E_1\\ E_2\end{pmatrix} = \frac{1}{\sqrt{2r}}\mathrm{Re}\sum_{k=1}^{3}\begin{Bmatrix}r_k\\ -s_k\end{Bmatrix}\frac{h_k}{\sqrt{\cos\theta+\mu_k\sin\theta}} \tag{A.3}$$

$$\begin{pmatrix}u_1\\ u_2\\ \phi\end{pmatrix} = \sqrt{2r}\mathrm{Re}\sum_{k=1}^{3}\begin{Bmatrix}p_k\\ q_k\\ -r_k\end{Bmatrix}h_k\sqrt{\cos\theta+\mu_k\sin\theta} \tag{A.4}$$

where μ_k $(k = 1, 2, 3)$ is the root of characteristic equation, and

$$h_k = \sqrt{a}[\Lambda_{k1}\sigma_{22}^{\infty} - \Lambda_{k2}\sigma_{12}^{\infty} - \Lambda_{k3}(D_2^{\infty} - D_2^0)] \tag{A.5}$$

where σ_{22}^{∞}, σ_{12}^{∞} and D_2^{∞} are the far-field loadings in (X_1, X_2) coordinate that are easily calculated from the far-field loadings $\sigma_{22}^{\prime\infty}$, $\sigma_{12}^{\prime\infty}$ and $D_2^{\prime\infty}$ in (X_1', X_2') coordinate. Moreover,

$$\Lambda = [\Lambda_{kj}] = \frac{1}{\Delta}\begin{pmatrix} \mu_2\lambda_3 - \mu_3\lambda_2 & \lambda_2 - \lambda_3 & \mu_3 - \mu_2 \\ \mu_3\lambda_1 - \mu_1\lambda_3 & \lambda_3 - \lambda_1 & \mu_1 - \mu_3 \\ \mu_1\lambda_2 - \mu_2\lambda_1 & \lambda_1 - \lambda_2 & \mu_2 - \mu_1 \end{pmatrix} \tag{A.6}$$

$$\Delta = (\lambda_2 - \lambda_3)\mu_1 + (\lambda_3 - \lambda_1)\mu_2 + (\lambda_1 - \lambda_2)\mu_3 \tag{A.7}$$

$$p_k = a_{11}\mu_k^2 + a_{12} - a_{13}\mu_k + \lambda_k(b_{11}\mu_k - b_{21}) \tag{A.8}$$

$$q_k = (a_{12}\mu_k^2 + a_{22} - a_{23}\mu_k + \lambda_k b_{12}\mu_k - \lambda_k b_{22})/\mu_k \tag{A.9}$$

$$r_k = -b_{11}\mu_k^2 - b_{12} + b_{13}\mu_k + \lambda_k(d_{11}\mu_k - d_{21}) \tag{A.10}$$

$$s_k = b_{21}\mu_k^2 + b_{22} - b_{23}\mu_k - \lambda_k(d_{12}\mu_k - d_{22}) \tag{A.11}$$

$$\lambda_k = \frac{b_{11}\mu_k^3 - (b_{21} + b_{13})\mu_k^2 + (b_{12} + b_{23})\mu_k - b_{22}}{d_{11}\mu_k^2 - 2d_{12}\mu_k + d_{22}} \tag{A.12}$$

a_{ij}, b_{ij} and d_{ij} $(i, j = 1, 2)$ are elastic, piezoelectric and dielectric constants, respectively, when the (X_1, X_2) coordinate system is employed and generally their values vary depending on crack oriented angle β. By using these, the constitutive equation for plane stress or plane strain problem under the (X_1, X_2) coordinate system can be expressed as

$$\begin{Bmatrix} \varepsilon_{11} \\ \varepsilon_{22} \\ 2\varepsilon_{12} \end{Bmatrix} = \begin{pmatrix} a_{11} & a_{12} & a_{13} \\ a_{12} & a_{22} & a_{23} \\ a_{13} & a_{23} & a_{33} \end{pmatrix} \begin{Bmatrix} \sigma_{11} \\ \sigma_{22} \\ \sigma_{12} \end{Bmatrix} + \begin{pmatrix} b_{11} & b_{21} \\ b_{12} & b_{22} \\ b_{13} & b_{23} \end{pmatrix} \begin{Bmatrix} D_1 \\ D_2 \end{Bmatrix} \tag{A.13}$$

$$\begin{Bmatrix} E_1 \\ E_2 \end{Bmatrix} = -\begin{pmatrix} b_{11} & b_{12} & b_{13} \\ b_{21} & b_{22} & b_{23} \end{pmatrix} \begin{Bmatrix} \sigma_{11} \\ \sigma_{22} \\ \sigma_{12} \end{Bmatrix} + \begin{pmatrix} d_{11} & d_{12} \\ d_{12} & d_{22} \end{pmatrix} \begin{Bmatrix} D_1 \\ D_2 \end{Bmatrix} \tag{A.14}$$

In Eq. (A.5), electric displacement inside the crack D_2^0 is dependent upon electric boundary conditions on crack surface. The well-known condition called exact boundary condition (Sosa and Khutoryansky, 1996; Zhang et al., 1998) is given as, on a defect surface,

$$D_n = D_n^0 = \kappa_0 E_n^0 = -\kappa_0 \frac{\Delta\phi}{\Delta u_n}, \quad \phi = \phi^0 \tag{A.15}$$

where superscript 0 and subscript n refer the quantities in the cavity and the normal component of the quantities, respectively. In this condition, as the defect approaches a crack of $\rho = 0$,

$$D_2^0 = \frac{\mathrm{Im}\sum_{k=1}^{3} r_k(-\Lambda_{k1}\sigma_{22}^{\infty} + \Lambda_{k2}\sigma_{12}^{\infty})}{Im\sum_{k=1}^{3} r_k\Lambda_{k3}} + D_2^{\infty} \tag{A.16}$$

It was found that Eq. (A.16) finally becomes the same as that for permeable boundary condition (Parton, 1976; Mikhailov and Parton, 1990) because dielectric inclusion phase physically vanishes when a void approaches an ideal crack. Another condition called Hao and Shen type boundary condition (Hao and Shen, 1994) is given as

$$D_2^+ = D_2^-, \quad D_2^+(u_2^+ - u_2^-) = -\kappa_0(\phi^+ - \phi^-) \tag{A.17}$$

where superscripts + and − denote the quantities on the upper and lower crack surfaces, respectively. Under Hao and Shen type boundary condition, the following solution for D_2^0 can be obtained:

$$D_2^0 = \kappa_0 \frac{\mathrm{Im}\sum_{k=1}^{3} r_k[\Lambda_{k1}\sigma_{22}^{\infty} - \Lambda_{k2}\sigma_{12}^{\infty} - \Lambda_{k3}(D_2^{\infty} - D_2^0)]}{\mathrm{Im}\sum_{k=1}^{3} q_k[\Lambda_{k1}\sigma_{22}^{\infty} - \Lambda_{k2}\sigma_{12}^{\infty} - \Lambda_{k3}(D_2^{\infty} - D_2^0)]} \tag{A.18}$$

where κ_0 is dielectric constant of the inclusion. For impermeable crack (Pak, 1992; Suo et al., 1992), D_2^0 becomes 0.

References

Chue, C.H., Weng, S.M., 2005. Fracture analysis of piezoelectric materials with an arbitrarily oriented crack using energy density theory. Comput. Struct. 83, 1251–1265.

Hao, T.-H., Shen, Z.-Y., 1994. A new electric boundary condition of electric fracture mechanics and its applications. Eng. Fract. Mech. 47, 793–802.

McHenry, K.D., Koepke, B.G., 1983. Electric fields effects on subcritical crack growth in PZT. Fract. Mech. Ceram. 5, 337–352.

Mikhailov, G.K., Parton, V.Z., 1990. Electromagnetoelasticity. Hemisphere, New York.

Nam, B.G., Liu, R., Tsuchida, S., Watanabe, K., 2007. Applicability of crack energy density (CED) to fracture strength evaluation of piezoelectric ceramics. Mater. Sci. Eng. A. 449–451, 343–347.

Nam, B.G., Watanabe, K., 2007. Crack energy density and energy release rate for piezoelectric material. Int. J. Solids Struct. 44, 3904–3919.

Nam, B.G., Watanabe, K., 2008. Effect of electric boundary conditions on crack energy density and its derivatives for piezoelectric material. Eng. Fract. Mech. 75, 207–222.

Pak, Y.E., 1992. Linear electro-elastic fracture mechanics of piezoelectric materials. Int. J. Fract. 54, 79–100.

Park, S.B., Sun, C.T., 1995. Fracture criteria for piezoelectric ceramics. J. Am. Ceram. Soc. 78, 1475–1480.

Parton, V.Z., 1976. Fracture mechanics of piezoelectric materials. Acta Astronaut. 3, 671–683.

Sosa, H.A., Khutoryansky, N., 1996. New developments concerning piezoelectric materials with defects. Int. J. Solids Struct. 33, 3399–3414.

Suo, Z., Kuo, C.M., Barnett, D.M., Willis, J.R., 1992. Fracture mechanics for piezoelectric ceramics. J. Mech. Phys. Solids 40, 739–765.

Utsunomiya, N., 1992. Ph.D. thesis, The University of Tokyo.

Watanabe, K., Shiomi, H., 1984. Extension of crack energy density concept to arbitrary direction and energy release rate to non-self-similar crack growth. Bull. JSME 27 (228), 1077–1084.

Xu, X.-L., Rajapakse, R.K.N.D., 1999. Analytical solution for an arbitrarily oriented void/crack and fracture of piezoceramics. Acta Mater. 47 (6), 1735–1747.

Xu, X.-L., Rajapakse, R.K.N.D., 2001. On a plane crack in piezoelectric solids. Int. J. Solids Struct. 38, 7643–7658.

Zhang, T.-Y., Qian, C.-F., Tong, P., 1998. Linear electro-elastic analysis of a cavity or a crack in a piezoelectric material. Int. J. Solids Struct. 35, 2121–2149.